**Title page**

# Sonic hedgehog medulloblastoma cells in co-culture with cerebellar organoids converge towards *in vivo* malignant cell states

Max J. van Essen[1,2], Alina Nicheperovich[3], Benjamin Schuster-Böckler[3,4], Esther B. E. Becker[1,2] and John Jacob[1*]

[1]Nuffield Department of Clinical Neurosciences, University of Oxford, Oxford, OX3 9DU, United Kingdom

[2]Kavli Institute for Nanoscience Discovery, University of Oxford, Oxford, OX1 3QU, United Kingdom

[3]Ludwig Institute for Cancer Research, University of Oxford, Nuffield Department of Medicine Old Road Campus Research Building, Roosevelt Drive, Oxford OX3 7DQ, United Kingdom

[4]Big Data Institute, University of Oxford, Li Ka Shing Centre for Health Information and Discovery, Old Road Campus, Oxford OX3 7LF, United Kingdom

*Correspondence: john.jacob@ndcn.ox.ac.uk

**Abstract**

**Background**

In the malignant brain tumour sonic hedgehog medulloblastoma (SHH-MB) the properties of cancer cells are influenced by their microenvironment, but the nature of those effects and the phenotypic consequences for the tumour are poorly understood. The aim of this study was to identify phenotypic properties of SHH-MB cells that were driven by the non-malignant tumour microenvironment.

**Methods**

Human induced pluripotent cells (iPSC) were differentiated to cerebellar organoids to simulate the non-malignant tumour microenvironment. Tumour spheroids were generated from two distinct, long-established SHH-MB cell lines which were co-cultured with cerebellar organoids. We profiled the cellular transcriptomes of malignant and non-malignant cells by performing droplet-based single-cell RNA-sequencing (scRNA-seq). The transcriptional profiles of tumour cells in co-culture were compared with those of malignant cells cultured in isolation and with public SHH-MB datasets of patient tumours and patient-derived xenograft (PDX) models.

**Results**

SHH-MB cell lines in organoid co-culture adopted patient tumour-associated phenotypes and showed increased heterogeneity compared to monocultures. Sub-populations of co-cultured SHH-MB cells activated a key marker of differentiating granule cells, *NEUROD1* that was not observed in tumour monocultures. Other sub-populations expressed transcriptional determinants consistent with a cancer stem cell (CSC)-like state that resembled cell states identified *in vivo*.

**Conclusion**

For SHH-MB cell lines in co-culture, there was a convergence of malignant cell states towards patterns of heterogeneity in patient tumours and PDX models implying these states were non-cell autonomously induced by the microenvironment. Therefore, we have generated an advanced, novel *in vitro* model of SHH-MB with potential translational applications.

**Keywords**

sonic hedgehog medulloblastoma, medulloblastoma cell lines, single-cell transcriptomics, human induced pluripotent stem cells, human cerebellar organoids

## Introduction

Medulloblastoma (MB), a heterogeneous cerebellar tumour is the most common malignant brain tumour of childhood.[1] Molecular profiling has defined four major subtypes, of which a third of cases are driven by aberrant sonic hedgehog (SHH) signalling (SHH-MB).[2] During development, SHH acting as a mitogen promotes massive expansion of the upper rhombic lip-derived cerebellar granule cell population in the external granule layer (EGL).[3] Somatic or germ-line mutations and focal somatic copy number alterations in SHH pathway tumour suppressors or oncogenes are the commonest events leading to aberrant SHH pathway activation and tumorigenesis in granule progenitors.[2] Although multimodal standard-of-care treatment has improved MB outcomes, neurological and systemic sequelae are debilitating and there is a substantial risk of relapse.[2] A greater understanding of how tumours progress is essential to develop novel therapies that selectively ablate tumour cells while minimising toxicity.

In patients and mouse models, SHH-MB contains $SOX2^+$ tumour-propagating neural stem-like cells, equivalent to cancer stem cells (CSC) and more differentiated cells.[2] By hijacking mechanisms of self-renewal in neural stem cells (NSC) and pluripotent stem cells, CSC can replenish tumours in transplantation assays.[4] During mammalian neurogenesis, initial ubiquitous SOX2 expression in the early embryonic central nervous system attenuates as the balance shifts from self-renewal to differentiation.[5] By contrast, in SHH-MB persistent SOX2-expressing granule progenitor-derived CSC can reconstitute tumours after therapy and support a hierarchical model of tumorigenesis.[6] Furthermore, cross-talk between the microenvironment and malignant cells suggests that cell extrinsic factors could also influence brain tumour cell states.[4] However, the complexity of the *in vivo* tumour microenvironment poses a challenge in discerning the involvement of distinct non-malignant components.

To address how the microenvironment affects tumour progression, we sought to evaluate the phenotypes of SHH-MB cells using single-cell transcriptomics, under defined conditions

82 that we anticipated might simulate *in vivo* tumour growth. To this end we leveraged
83 cerebellar organoid differentiation from human induced pluripotent stem cells (hiPSC)
84 through their co-culture with two SHH-MB cell lines [7] that were compared with conventional
85 *in vitro* tumour cultures. Organoids can be grown in xeno-free culture medium and they
86 contain defined neuronal and glial cell types. Although lacking immune cells or blood
87 vessels, they provide more physiological conditions than conventional *in vitro* models
88 enabling the evaluation of tumour cell phenotypes in a simulated native
89 microenvironment.[8]
90
91 **Materials and Methods**
92 Organoid differentiation
93 Cerebellar organoid differentiation was performed as described previously.[9] In brief, human
94 iPSC line AH017-3 cells [10] were detached by incubation with pre-warmed TrypLE for 5
95 minutes. Cells were collected by centrifugation and resuspended in induction medium (50%
96 IMDM, 50% F12, 7ug/mL Insulin, 5mg/mL BSA, 1X Chemically defined Lipid concentrate,
97 450uM Monothioglycerol, 15ug/mL Apo-transferrin, 1X Penicillin/Streptomycin) at a final
98 concentration of 100,000 cells/ml. 10,000 cells per well were plated in an ultra-low-
99 attachment V-bottom 96 well plate and returned to the incubator. After two days, FGF2 was
100 added at a final concentration of 50 ng/ml. One-third medium change was performed at day
101 7 and full medium change at day 14. On this day, the organoids were also transferred into a
102 low-attachment 48-well plate. On day 21, medium was changed to differentiation medium
103 (Neurobasal + 1% N2 supplement + 1% GlutaMAX + 1X Penicillin/Streptomycin) and
104 subsequent full medium changes were performed on days 28 and 35. After day 35, medium
105 was changed twice/week.
106
107 Medulloblastoma cell lines, tumour spheroids and organoid-tumour spheroid co-culture
108 DAOY-GFP cells (gift from Vincenzo D'Angiolella, DAOY cell line originally purchased from
109 ATCC) were grown in monolayer culture in MEM, 1% GlutaMAX, 1X Penicillin/Streptomycin
110 and 1% FBS (cell line authentication in Supplementary Table 1). ONS-76-Luciferase-GFP cells
111 (gift from Louis Chesler; ONS-76 cell line originally purchased from JCRB Cell Bank by Steven
112 Clifford) were grown in monolayer culture in RPMI + 1% GlutaMAX + 1X
113 Penicillin/Streptomycin + 1% FBS (Supplementary Table 1). Medium was changed twice per

114 week. To generate tumour spheroids, cells were detached by incubation with pre-warmed
115 TrypLE for 5 minutes and collected by centrifugation. Cells were resuspended in
116 differentiation medium at a concentration of 200,000 cells/ml and plated in an ultra-low-
117 attachment V-bottom 96-well plate at 20,000 cells per well. In preparation for cerebellar
118 organoid-tumour spheroid coculture, one week prior to the start of co-culture, tumour
119 spheroids were generated as described above. One tumour spheroid was placed with one
120 day 35 organoid in a low-attachment 24-well plate in identical differentiation medium. To
121 facilitate fusion of the tumour spheroid and the organoid, the plate was incubated for two
122 days at a 45-degree angle. Medium was changed twice per week and the cells were
123 maintained in co-culture, alongside tumour spheroid and tumour monolayer cultures for a
124 further 25 days (Fig. 1A).
125
126 Single cell isolation
127 Day 60 organoids and organoid-tumour co-culture samples were collected using a wide bore
128 pipette tip and placed in a 6-well plate. Five tumour spheroid-organoid co-cultures for each
129 cell line and a similar number of control organoids were each cut in four pieces and placed
130 in an Eppendorf tube. After removal of excess medium, 200 μl of pre-warmed (to 37°C)
131 Neuron isolation enzyme was added and the tube was placed in a 37°C water bath.
132 Organoids were incubated with the enzyme for 30 minutes with intermittent agitation. The
133 enzyme was removed and organoids were washed once with HHGN medium (HBSS + 2.5mM
134 HEPES + 35mM Glucose + 4mM $NaHCO_3$). Organoids were then dissociated in differentiation
135 medium by gentle trituration. Afterwards, the cell suspension was enriched for viable cells
136 using the dead cell removal kit (Miltenyi Biotec) following the manufacturers protocol. Cell
137 viability was determined using Trypan Blue staining and counted using an automated cell
138 counter (Applied Biosystems Countess 3). Cells were centrifuged at 300 x *g* for 5 minutes
139 and resuspended in the appropriate volume of resuspension buffer (HBSS + 0.04% BSA) to a
140 final concentration of 2000 cells/μl before proceeding with single-cell RNA sequencing.
141 Thirty tumour spheroids were collected using a wide bore pipette tip and placed in an
142 Eppendorf tube. Excess medium was removed and 200 μl of pre-warmed Neuron isolation
143 enzyme (Gibco) was added. The tube was placed in a 37°C water bath for 20 minutes and
144 agitated every 5 minutes. Subsequent processing was performed following the same steps

145 as described above. DAOY and ONS-76 cell monolayer cultures were dissociated by
146 incubation with pre-warmed TrypLE for 5 minutes. TrypLE was then diluted in PBS before
147 centrifugation at 400 x *g* for 5 minutes to collect the cells. Cells were washed once in
148 differentiation medium before processing as described above. Single cell barcoding and
149 reverse transcription of poly-A mRNA was performed using the 10X Chromium controller (3'
150 version 3.1 chemistry) and sequencing of single-cell libraries was performed on an Illumina
151 NovaSeq6000 sequencing system according to the manufacturer's instructions.
152
153 Data pre-processing and analysis
154 Initial sequencing data exploration was performed using Cell Ranger v6.1.1. For each dataset
155 we removed cells with 10% or higher mitochondrial gene expression [11] and genes expressed
156 in fewer than 10 cells. Downstream analysis largely implemented the workflow of Seurat v4,
157 using the 'sctransform' modelling framework, which corrects counts for each gene in a cell
158 by regressing out sequencing depth.[12] The difference between G2M and S phase scores was
159 regressed out so that differences in cell cycle phase among proliferating cells was
160 eliminated, while at the same time retaining signals separating cycling and non-cycling cells.
161 For differential gene expression testing between clusters a Bonferroni-corrected p-value <
162 0.05 was considered significant. To perform gene set enrichment analysis, we first used the
163 R package PRESTO which performs a fast Wilcoxon rank sum test on the Seurat clusters.[13]
164 We then tested functional enrichment of Seurat clusters of interest using gene sets from
165 MsigDB and the fgsea package.[14,15] Visualisation of pathway enrichment analysis was
166 performed using g:Profiler to search for Gene Ontology pathways that were significantly
167 enriched in a gene list before visualising the results using EnrichmentMap in Cytoscape.[16,17]
168 Pathway gene sets with fewer than three genes and more than 350 genes were excluded in
169 line with the default g:Profiler and Cytoscape workflows. For g:Profiler, a Benjamini-
170 Hochberg false discovery rate adjusted p-value of < 0.05 was considered significant.
171 Pseudotime analysis was conducted using Monocle 3.[18] Dataset integrations were, in
172 general, performed using standard workflows in Seurat v4, except when integrating
173 malignant cell populations (see Fig. 5) where we observed strong blending of distinct
174 malignant cell states. Instead, we used the fastMNN algorithm,[19] which was found to
175 preserve biological differences between cancer cell populations, while ensuring effective
176 batch correction.[20]

177 Statistical Analysis

178 Statistical significance testing was performed using R.

179

180 **Results**

181 Malignant tumour spheroids of ONS-76 cells or DAOY cells, which harbour wild type and
182 mutant copies of *TP53*, respectively were co-cultured with non-malignant cerebellar
183 organoids differentiated from human iPSC (Fig. 1A; Supplementary Fig. S1A). As controls,
184 tumour cells were grown as monolayers or tumour spheroids and non-malignant organoids
185 were cultured in isolation. After 25 days in co-culture, all cells were dissociated and
186 processed for single-cell RNA sequencing (scRNA-seq) on the 10X Chromium platform. After
187 filtering the dataset in accordance with our quality control thresholds we selected 13,534
188 cells for further analysis (Supplementary Fig. S1B – E; Supplementary Table 2). We used
189 Seurat to visualise the relationship between samples by clustering and projected cells in a
190 common UMAP space labelled according to their sample of origin (Supplementary Fig. S1F,
191 G). ONS-76 cells and DAOY cells cultured as monolayers or tumour spheroids formed well-
192 demarcated clusters. In contrast, there was extensive overlap of co-cultured cells with the
193 non-malignant organoid control, which was anticipated given the large numbers of cells
194 recovered belonging to organoid cellular subtypes. Only a handful of cells from the non-
195 malignant control organoid clustered with the exclusively malignant samples, confirming
196 that the clustering reflected biological differences between the samples. In the co-cultured
197 samples, several times the number of cells clustered with the malignant samples suggesting
198 the latter cells were malignant cells in co-culture.

199

200 **ONS-76 and DAOY cells cultured as monolayers or tumour spheroids were enriched for**
201 **proliferative, protein biosynthetic and wound healing processes**

202 We performed an integrated analysis of ONS-76 monolayer and tumour spheroid
203 transcriptomes in Seurat [12] and compared the transcriptional programmes of malignant cells
204 using functional enrichment analysis in the two conditions.[15] ONS-76 cells grown as
205 monolayers were enriched for Gene Ontology (GO) terms for cell cycle associated genes
206 (Supplementary Fig. S2A and Supplementary Table 3). In comparison, genes upregulated in
207 tumour spheroids were associated with altered cell morphology and wound healing for
208 example *IFITM3, IGFBP2, IGFBP5, STC1* and *SPARC* (Supplementary Fig. S2B – C and

209 Supplementary Table 3) consistent with an epithelial-to-mesenchymal transition (EMT) state
210 and tumour stroma production.[21] Upon clustering of the ONS-76 tumour spheroid sample
211 (Supplementary Fig. S2D), expression of these genes was distributed over all clusters
212 (Supplementary Fig. S2E) supporting relative homogeneity of malignant cell states with
213 mostly arbitrary distinctions between clusters, with two exceptions. The first consisted of a
214 cluster of cycling cells, denoted 'cluster 4' that was marked by the expression of genes
215 including *MKI67*, *MYBL2*, *BIRC5* and *RRM2* consistent with a proliferative cell state
216 (Supplementary Fig. S2D, G). Although the same genes were expressed in the ONS-76
217 monolayer sample, they were not restricted to a single cluster (Supplementary Fig. S2I). A
218 second ONS-76 tumour spheroid cluster, 'cluster 0' expressed ribosomal genes and was
219 enriched for protein synthesis pathways (Supplementary Fig. S2D and Supplementary Table
220 4), which is a feature common to many cancers.[22] Less heterogeneity was evident in ONS-76
221 cells cultured as monolayers, which could be split into two clusters also distinguished by
222 their relative enrichment for ribosomal genes and protein synthesis (Supplementary Fig.
223 S2H; Supplementary Table 4). In comparison to ONS-76 tumour spheroids, expression of
224 proliferation genes spanned both clusters, although the proliferation signal of individual
225 cells was weaker (Supplementary Fig. S2H, lower panel).
226
227 Broadly similar findings were observed upon analysis of DAOY cells cultured as monolayers
228 and tumour spheroids. An integrated analysis of the cellular transcriptomes revealed
229 protein synthesis gene sets as the only significant enrichment (Supplementary Table 5) in
230 DAOY tumour spheroids. In common with ONS-76 cells, wound healing gene sets were also
231 upregulated, but in DAOY monolayers rather than in DAOY tumour spheroids. Furthermore,
232 there was a degree of enrichment in oncogenic signature gene sets that was statistically
233 non-significant for transcriptional responses of cerebellar granule progenitors to activation
234 by SHH, which acts as a mitogen for these cells (Supplementary Table 5).
235
236 Clustering of the DAOY tumour spheroid sample also revealed enrichment of protein
237 synthesis and cell cycle related pathways, respectively in two out of five DAOY tumour
238 spheroid clusters (Supplementary Fig. S2F; Supplementary Table 5). Therefore, in tumour
239 spheroids of both cell lines, those cells with a signature of enhanced proliferation were
240 restricted to specific clusters in UMAP space, suggesting an association with a distinct cell

241 state related to malignant cell proliferation. By contrast, DAOY monolayer cells that
242 expressed a proliferative signature were spread diffusely across multiple clusters in common
243 with ONS-76 monolayer cultured cells (Supplementary Fig. S2J). Although DAOY monolayer
244 cells formed more clusters than ONS-76 cells (six in DAOY monolayers compared to two in
245 the corresponding ONS-76 sample), only three out of six of the former clusters displayed
246 significant gene set enrichment. Of these, two clusters were enriched for protein synthesis
247 pathways and the remaining cluster was only significantly enriched for cell adhesion-related
248 gene sets, which is a hallmark of cancer (Supplementary Table 5).[23] Assessment of the
249 maturity of malignant cells from tumour spheroid and monolayer samples of both cell lines
250 revealed they expressed the granule cell markers, *MEIS1,*[24] *MEIS2* [25] and *JKAMP* [26]
251 (Supplementary Fig. S2K). However, *CNTN1* which marks differentiating granule cells [27] was
252 selectively expressed only in ONS-76 samples, suggesting the maturation of DAOY cells was
253 relatively impaired (Supplementary Fig. S2K).
254
255 **ONS-76 cells in co-culture, but not in monolayers or tumour spheroids expressed**
256 ***NEUROD1***
257 To determine whether malignant cells grown in a non-malignant organoid
258 microenvironment led to altered tumour cell phenotypes, we clustered the ONS-76 sample
259 in co-culture and plotted the UMAP projection, comparing the clusters obtained with those
260 in the non-malignant control organoid (Fig. 1B; Supplementary Fig. S3A). The manual
261 annotations of non-malignant cells were highly similar to our earlier annotations of day 90
262 organoids.[28] None of the clusters of malignant cells in co-culture were identified as having a
263 match in the control organoid.
264
265 In the control organoid, granule neurons could be defined by their co-expression of
266 *NEUROD1*, *RTN1* and *RBFOX3* (Fig. 1C).[26] In the co-culture condition also, a cluster of cells
267 co-expressing these genes could be identified consistent with non-malignant granule
268 neurons (Fig. 1D). Additionally, a distinct cell cluster located adjacent to non-malignant
269 granule neurons in UMAP space could be distinguished from the latter cells by their
270 expression of *NEUROD1* only, which we labelled 'ONS76_cluster_3' (Fig. 1D; Supplementary
271 Fig. S3B; Supplementary Table 6). Furthermore, upon computational integration of ONS-76

272 samples malignant *NEUROD1*$^{+}$ cells were absent in ONS-76 monolayers and tumour
273 spheroids (Fig. 1E) and only very few were present in the DAOY samples (Fig. 1E, F).
274
275 Although *NEUROD1* marks post-mitotic granule neurons in mouse,[29] in humans this gene is
276 also expressed in cycling granule progenitors.[30] Gene set enrichment analysis of
277 'ONS76_cluster_3' revealed GO terms associated with cycling cells (Fig. 1G; Supplementary
278 Fig. S3C). By contrast, the cluster annotated as 'Granule neurons' in the non-malignant
279 organoid in co-culture and in the control organoid were enriched for terms associated with
280 differentiated neurons (Fig. 1I; Supplementary Fig. S3E, F). To validate these findings, we
281 computationally examined the cell cycle phase associated with *NEUROD1* expression in non-
282 malignant and malignant cells.[12] In the cluster annotated as 'Granule neurons' in the control
283 organoid (Fig. 1C), the fraction of *NEUROD1*$^{+}$ cells that were in G1 phase was 0.60, in G2/M
284 phase the fraction was 0.17 and the S phase fraction was 0.23. However, in ONS-76 cells in
285 co-culture the fraction of *NEUROD1*$^{+}$ cells in 'ONS76_cluster_3' in G1 phase was smaller
286 (0.38), and the fraction of cells in G2/M and S phases was higher (0.30 and 0.32,
287 respectively; $p = 5.925 \times 10^{-12}$ Chi-squared test). Therefore, ONS-76 cells activated
288 *NEUROD1,* a key molecular determinant of granule cell identity only when embedded in a
289 more physiological microenvironment, but its expression was less tightly coupled to other
290 cellular processes that imparted a differentiated neuronal identity. By comparison, analysis
291 of patient SHH-MB scRNA-seq public datasets showed that they also expressed *NEUROD1*
292 (Supplementary Fig. 4A-E) [31,32] and that for one of the datasets [31] most of these cells were in
293 G1 phase (range 0.59 – 0.69). Consistent with maturation of malignant cells, patient
294 tumours also expressed *RBFOX3* and *RTN1* (Supplementary Fig. S4A-E). Given the absence of
295 *NEUROD1* upregulation in DAOY cells in co-culture, we analysed its expression in two *TP53*
296 mutant SHH-MB in a second public MB scRNA-seq dataset to test for an association
297 between presence of the mutation and *NEUROD1* expression *in vivo*.[32] The tumours varied
298 widely in their expression of *NEUROD1* displaying both elevated and minimal expression
299 (Supplementary Fig. S4D). Therefore, absence of *NEUROD1* expression in *TP53* mutant DAOY
300 cells in tumour spheroid-organoid co-culture was not inconsistent with *in vivo* findings.
301
302 A second, smaller cluster of ONS-76 tumour cells in co-culture, 'ONS76_cluster_10' was
303 identified by differential upregulation of *HOXB2* and *POU3F2*, in common with multiple non-

304 CNS cancers including leukaemia, lung and breast cancer (Fig. 1H; Supplementary Table
305 6).[33,34] Cells in this cluster also expressed *MEIS1*, which is expressed by differentiating
306 granule cells [35] and *HOXB-AS1*, which is a member of a large family of non-coding transcripts
307 that are abnormally expressed in a wide range of cancers.[36] Consistent with the expression
308 of *MEIS1*, gene set enrichment analysis suggested this cluster contained mature cells
309 (Supplementary Fig. S3G, H). Overall, subpopulations of malignant cells expressed *in vivo*
310 markers of differentiation when they were surrounded by the more physiologic
311 microenvironment of the organoid.
312
313 **A sub-population of DAOY cells in co-culture expressed multiple cancer stem cell-like**
314 **markers**
315 The analysis of the DAOY tumour spheroid-organoid co-culture sample resulted in clustering
316 of DAOY tumour cells into three distinct groups in UMAP space designated as
317 'DAOY_cluster_9', 'DAOY_cluster_13', 'DAOY_cluster_14' (Fig. 2A). Highly distinctive,
318 differential expression of specific markers of these putative malignant clusters was apparent
319 exemplified by *PTCH1, MEIS1, POU3F4, FGFBP3, TWIST1* and *LHX9* that displayed low or no
320 expression in non-malignant cells in co-culture and in the control organoid (Fig. 2B, D and
321 Supplementary Table 6). Noting that *POU3F4* and *FGFBP3* have been linked to a neural stem
322 cell (NSC) identity,[37,38] we compared DAOY cells in co-culture with the DAOY tumour
323 spheroid sample for expression of NSC markers (Supplementary Fig. S5A). Multiple NSC
324 markers were upregulated in DAOY cells in co-culture including *SOX2*, *NES*, *FABP7* and *MSI1*
325 (Fig. 2C). A similar trend was observed for ONS-76 cells in the three conditions, although the
326 upregulation of these NSC markers in ONS-76 cells in co-culture was not as great (Fig. 2E).
327
328 The upregulation of NSC markers in malignant cells in our co-culture model is reminiscent of
329 mouse models of SHH-MB, in which persistent SOX2-expressing granule cells designated as
330 cancer stem cells (CSC) drive tumour formation and relapse.[6,39] We therefore focused our
331 analysis on further characterising the transcriptional profile of these cells. More granular
332 analysis at the level of individual malignant clusters revealed striking differences in the
333 expression of factors known to regulate *SOX2* compared to DAOY cells cultured in other
334 conditions and ONS-76 cells (Fig. 3A).[40] Only a single DAOY cluster in co-culture,
335 'DAOY_cluster_9' expressed multiple members of the *SOX2* regulatory network consisting of

336 *POU3F2*, *ZIC2*, *OTX2*, *GLI2* and *SOX2* itself (Fig. 3B). This combinatorial pattern of gene
337 expression was not observed in ONS-76 cells in co-culture (Fig. 3C), nor in tumour spheroid
338 or monolayer samples of either cell line (Fig. 3D), or in non-malignant organoid cells (Fig.
339 3E). The co-expression of these markers in subpopulations of DAOY cells in co-culture
340 suggested these cells adopted a new cell state in the presence of a non-malignant
341 microenvironment.
342
343 We hypothesised there could be an ontological relationship between the distinct DAOY cell
344 states identified in co-culture. In particular, the UMAP plot of DAOY cells in co-culture (Fig.
345 2A) suggested 'DAOY_cluster_9' and 'DAOY_cluster_13' cells occupied opposite ends of a
346 single trajectory. A pseudotime analysis supported the notion that 'DAOY_cluster_9' could
347 undergo a progressive transition to a 'DAOY_cluster_13' cell state (Fig. 3F). Pathway
348 enrichment analysis was consistent with the pseudotime analysis and showed that
349 'DAOY_cluster_9' cells were enriched for GO terms associated with a proliferative state (Fig.
350 3G; Supplementary Table 7), whereas 'DAOY_cluster_13' was enriched for neuronal
351 differentiation terms (Fig. 3H and Supplementary Table 7). The last cluster,
352 'DAOY_cluster_14' was transcriptionally less similar to the other DAOY clusters (Fig. 2A).
353 Enriched pathways for this cluster related to Notch and Hedgehog signalling, translation
354 regulation and included extracellular matrix composition and wound healing gene sets in
355 common with tumour cells cultured in isolation (Fig. 3I; Supplementary Table 7).
356
357 **CSC-like cells with a molecular profile resembling DAOY tumour cells in co-culture are**
358 **present in patient SHH-MB**
359 We analysed the expression of the *SOX2* regulatory network in a public scRNA-seq dataset
360 of patient SHH-MB.[31] Upon clustering tumour cells in Seurat [12] a single cluster in one of
361 three SHH-MB tumours expressed a highly similar network in which *OTX2* was replaced by
362 expression of another member of the regulatory network, *SRRT* (Fig. 3A and Fig. 4A).[40]
363 Furthermore, in one of two PDX models of SHH-MB from the same dataset,[31] a single
364 cluster expressed a common network, consisting of *POU3F2*, *OTX2*, *SRRT*, *GLI2* and *SOX2*
365 (Fig. 4A). Given these differences, and to determine the prevalence and identity of cells
366 expressing a signature of a *SOX2* regulatory network, we analysed a larger dataset of patient
367 SHH-MB.[32] Initial analysis of the data showed upregulation of all the aforementioned genes

368 in malignant cells compared to the non-malignant microenvironment (Fig. 4B). By contrast,
369 co-expression of these genes was weaker in other MB subtypes (Supplementary Fig. S5B).
370 Clustering the individual SHH-MB tumours showed that in 7/8 samples two to four clusters
371 emerged per tumour. One or more of these clusters expressed a *SOX2* regulatory network
372 that was highly similar to the regulatory network in DAOY cells in co-culture (Fig. 4C, D;
373 Supplementary Fig. S5C – H). The proportion of malignant cells expressing this signature
374 ranged from 4.2% to 20.3% (median 8.8%) in this dataset.[32] Quantification of the gene
375 signature across MB subtypes showed enrichment in SHH-MB tumours (Fig. 4E).
376 Furthermore, *TP53* mutation status (n = 2 *TP53* mutant SHH-MB tumours) was unrelated to
377 the occurrence of the gene signature. These data confirmed that the patterns of gene
378 expression in DAOY cells in co-culture were not simply an artifact related to our culture
379 conditions, and instead suggested DAOY cells mirrored a CSC-like state found *in vivo*.
380
381 **Greater transcriptional similarity of DAOY and ONS-76 cells in co-culture to patient SHH-**
382 **MB**
383 Encouraged by the transcriptional evidence suggesting tumour heterogeneity resembling
384 SHH-MB *in vivo* in our organoid co-culture model, we assessed the transcriptional similarity
385 of our model to patient tumours and PDX models. Therefore, we compared the
386 computational integration of DAOY and ONS-76 tumour cells in co-culture and PDX models
387 with patient SHH-MB tumours. We did not use canonical correlation implemented in Seurat
388 for this part of the analysis because this algorithm excessively blends distinct cancer cell
389 states.[20] Instead, we employed the fastMNN algorithm,[41] which performed well in an earlier
390 benchmarking study of tumour datasets [20] to integrate three public SHH-MB patient single-
391 cell datasets.[31] Upon projection in UMAP space two major clusters emerged to which all
392 three tumours contributed (Fig. 5A). Two SHH-MB PDX tumours [31] blended well with the
393 patient tumours but showed greater mixing with one of the two major clusters, suggesting
394 these PDX models did not recapitulate the full extent of transcriptional diversity of the
395 patient tumours (Fig. 5B, C). Whereas DAOY and ONS-76 cells in co-culture, as expected,
396 were less similar to patient tumours (Fig. 5D, E), in comparison with tumour spheroids of
397 either cell line far greater similarity was evident (Fig. 5F, G). We also computed a 'mixing
398 metric' to quantify how similar these datasets were after integration (Fig. 5H and
399 Supplementary Table 8).[42] Patient tumours scored the highest on this metric, followed

400 closely by PDX tumours. Strikingly, our tumour spheroid organoid co-culture models also
401 performed well, in contrast to tumour spheroid models.
402
403 **Discussion**
404 Human cerebellar organoid-based *in vitro* models have the potential to recapitulate patient
405 MB more faithfully compared to conventional in vitro models.[43] Here, we tested the
406 importance of the non-malignant microenvironment in regulating malignant cell states by
407 comparing the phenotypes of two long-established SHH-MB lines grown in co-culture or
408 conventionally. Compared to conventional *in vitro* models, we detected greater maturity of
409 malignant cells in co-culture. In particular, a subpopulation of ONS-76 cells activated the
410 expression of *NEUROD1*, a canonical marker of granule cells, only upon co-culture.
411 Additionally, a subpopulation of DAOY cells in co-culture expressed CSC-like markers and
412 pseudotime and functional enrichment analyses were concordant attesting to their capacity
413 for maturation into cells with neuronal features. The expression of CSC-like markers and
414 upregulation of neuronal differentiation genes by malignant cells in co-culture revealed the
415 emergence of cell states that were not observed in tumour cells cultured in isolation, under
416 our conditions. Given that similar cell states are found in mouse models, PDX models and
417 upon patient tumour molecular profiling,[6,31,39,44] we further demonstrated the convergence
418 of two SHH-MB cell lines towards *in vivo* cellular phenotypes. Therefore, the
419 microenvironment can non-cell autonomously regulate SHH-MB cell states.
420
421 The fact that malignant cell phenotypes in tumour spheroid-organoid co-culture were
422 similar to those seen *in vivo* in patient tumours and PDX models (Fig. 1D, E; Fig. 3B; Fig. 4;
423 Fig. 5) confirms the validity of our model in recapitulating patient tumours better than
424 conventional *in vitro* models. Moreover, our findings suggest that the consensus view that
425 these cell lines are poorly representative of patient tumours does not hold true when these
426 malignant cell lines are cultured in a more physiological context. The emergence of new cell
427 states in these long-established SHH-MB cell lines that was not evident in monolayer or
428 tumour spheroid culture conditions was striking, more so given the relatively short duration
429 (25 days) of co-culture. The immediate cause of these rapid phenotypic changes is likely to
430 be transcriptional plasticity, reflecting functional intra-tumour heterogeneity that is shared
431 by diverse malignant tumours.[45]

432

433 Malignant granule cells can differentiate in patient SHH-MB and in mouse models of this
434 disease.[31,32,44,46,47] Interestingly, the activation of *NEUROD1* in SHH-MB patient samples
435 showed no dependency on *TP53* mutational status (Supplementary Fig. S4D), suggesting
436 that differentiation processes can still be initiated in the presence of somatic *TP53*
437 mutations.[48] *NEUROD1* was upregulated in a sub-population of ONS-76 cells in tumour
438 spheroids in co-culture with organoids compared to tumour monocultures (Fig. 1D, E). In
439 both healthy and malignant cells, expression of *NEUROD1* was associated with actively
440 cycling cells and cells with neuronal features (Fig. 1G, I; Supplementary Fig. S3C – F).
441 Interestingly, however, in the malignant sub-population, upregulation of *NEUROD1* was not
442 as tightly coupled with neuronal differentiation compared to non-malignant granule cells.
443 These differences could reflect divergence of the properties of ONS-76 cells over an
444 extended period *in vitro*, favouring the survival of cycling cells over more differentiated
445 cells. Recent analysis of human granule cell ontogeny has demonstrated that, in contrast to
446 mouse, these cells express *NEUROD1* during their cycling phase.[30] The expression of this
447 gene in a smaller proportion of non-malignant cycling granule precursors is consistent with
448 the latter finding and further validates our cerebellar organoid model.
449

450 Our analysis showed that the DAOY CSC-like cells present in co-culture were enriched for
451 pathways related to the cell cycle, which suggested they were proliferative (Fig. 3G and
452 Supplementary Fig. S3C). Moreover, closely similar or equivalent cell states as defined by
453 expression of the *SOX2* regulatory network were present in a majority of samples across two
454 published scRNA-seq datasets (Fig. 4 and Supplementary Fig. S5C – H).[31,32] Reasons for the
455 differences in the expressed members of the *SOX2* regulatory network in CSC-like
456 subpopulations are unclear. Differences could relate to redundancy of distinct *SOX2*
457 regulators or reflect divergence of functional states within CSC-like populations, associated
458 with, for example, different proliferation rates and sensitivity to therapy. The traditional
459 view is that CSC are rare, slow-cycling cells that are relatively quiescent compared to other
460 malignant cells, and such tumour-initiating cells were identified in a SHH-MB mouse
461 model.[6,39] The proportion of CSC-like cells in the scRNA-seq dataset we analysed [32] was up to
462 ~20% with a median close to 10%, suggesting these cells might be more common than
463 previously thought. Moreover, in another brain tumour, glioma, stem cells have also been

464 reported to be proliferative, supporting the view that CSC states are non-uniform.[4] Future
465 functional studies are needed to determine if the SHH-MB cells with the signature we
466 identified meet the standard for stemness in *in vivo* limiting dilution assays. Pseudotime and
467 functional enrichment analyses were consistent and suggested these cells underwent a
468 maturation process, associated with a continuum of cell states that led to the acquisition of
469 neuron-like features (Fig. 3F – H). Furthermore, we discounted the possibility that the
470 emergence of a CSC-like state in DAOY cells was caused by the *TP53* mutation because of
471 the prevalence of a CSC-like state in patient SHH-MB analysed here that were wild type for
472 *TP53* and the expression of NSC markers in ONS-76 cells in tumour spheroid-organoid co-
473 culture (Fig. 2E).
474
475 In our co-culture model, single or multiple constituents of the non-malignant
476 microenvironment could induce the emergent phenotypic states of SHH-MB cells.
477 Regulatory interactions between malignant and non-malignant components that exploit
478 local signalling networks are a well-established mechanism for tumour cells to gain a growth
479 advantage.[49] Microenvironmental factors implicated in these signalling networks *in vivo*
480 include stromal cells, blood and lymphatic vessels, immune-inflammatory cells and
481 extracellular matrix (ECM). Of these, ECM is the only one of these factors represented in our
482 co-culture model and has a well-recognised role in tumour progression.[50] Whether other
483 components of the microenvironment in our model, namely progenitors, neurons, glia, roof
484 plate or choroid plexus can produce malignant cell state-reprogramming signals is unclear.
485 Identification of this factor(s) in future could open new therapeutic options.
486
487 **Funding**
488 This work was supported by Cancer Research UK (CRUK) grant number C2195/A28699,
489 through a CRUK Oxford Centre Clinical Research Training Fellowship to MvE and by a
490 Medical Research Council award to JJ (award number: MR/V037730/1). BSB is funded by the
491 Ludwig Institute for Cancer Research.
492
493 **Conflicts of Interest**
494 The authors declare they have no conflict of interest.
495

496 **Authorship**

497 JJ conceived the project and JJ and MvE designed experiments. MvE performed the
498 experimental work and AN and JJ performed data analysis. EB and BSB provided advice on
499 experimental design and analysis. JJ wrote the manuscript with contributions from all the
500 authors.

501

502 **Data Availability**

503 scRNA-seq data have been deposited in the National Centre for Biotechnology Information
504 Gene Expression Omnibus (GEO) database and are publicly accessible through GEO
505 accession number GSE254917
506 (https://www.ncbi.nlm.nih.gov/geo/query/acc.cgi?acc=GSE254917). Analysis code is
507 available at https://github.com/jjacob12/carp_analysis50K/tree/main/PrePrint.

508

509 **Acknowledgements**

510 Computation used the Oxford Biomedical Research Computing (BMRC) facility, a joint
511 development between the Wellcome Centre for Human Genetics and the Big Data Institute
512 supported by Health Data Research UK and the NIHR Oxford Biomedical Research Centre.
513 We thank Dr Jia-Ling Ruan (Department of Oncology, Medical Sciences Division, University
514 of Oxford) for preparing SHH-MB cell lines for authentication.

515

516 **References**

517

518 **1.** Dolecek TA, Propp JM, Stroup NE, Kruchko C. CBTRUS statistical report: primary brain
519 and central nervous system tumors diagnosed in the United States in 2005-2009.
520 *Neuro Oncol.* 2012; 14 Suppl 5(Suppl 5):v1-49.
521 **2.** Garcia-Lopez J, Kumar R, Smith KS, Northcott PA. Deconstructing Sonic Hedgehog
522 Medulloblastoma: Molecular Subtypes, Drivers, and Beyond. *Trends Genet.* 2021;
523 37(3):235-250.
524 **3.** Wechsler-Reya RJ, Scott MP. Control of neuronal precursor proliferation in the
525 cerebellum by Sonic Hedgehog. *Neuron.* 1999; 22(1):103-114.
526 **4.** Gimple RC, Yang K, Halbert ME, Agnihotri S, Rich JN. Brain cancer stem cells:
527 resilience through adaptive plasticity and hierarchical heterogeneity. *Nat Rev Cancer.*
528 2022; 22(9):497-514.
529 **5.** Hagey DW, Klum S, Kurtsdotter I, Zaouter C, Topcic D, Andersson O, Bergsland M,
530 Muhr J. SOX2 regulates common and specific stem cell features in the CNS and
531 endoderm derived organs. *PLoS Genet.* 2018; 14(2):e1007224.

532 **6.** Selvadurai HJ, Luis E, Desai K, Lan X, Vladoiu MC, Whitley O, Galvin C, Vanner RJ, Lee
533 L, Whetstone H, Kushida M, Nowakowski T, Diamandis P, Hawkins C, Bader G,
534 Kriegstein A, Taylor MD, Dirks PB. Medulloblastoma Arises from the Persistence of a
535 Rare and Transient Sox2(+) Granule Neuron Precursor. *Cell Rep.* 2020; 31(2):107511.
536 **7.** Ivanov DP, Coyle B, Walker DA, Grabowska AM. In vitro models of medulloblastoma:
537 Choosing the right tool for the job. *Journal of Biotechnology.* 2016; 236:10-25.
538 **8.** van Essen MJ, Apsley EJ, Riepsaame J, Xu R, Northcott PA, Cowley SA, Jacob J, Becker
539 EBE. PTCH1-mutant human cerebellar organoids exhibit altered neural development
540 and recapitulate early medulloblastoma tumorigenesis. *Dis Model Mech.* 2024; 17(2).
541 **9.** van Essen MJ, Nayler S, Apsley EJ, Jacob J, Becker EBE. Cerebellar Modelling Using
542 Human Induced Pluripotent Stem Cells (hiPSCs). In: Sillitoe RV, ed. *Measuring*
543 *Cerebellar Function*. New York, NY: Springer US; 2022:1-21.
544 **10.** Handel AE, Chintawar S, Lalic T, Whiteley E, Vowles J, Giustacchini A, Argoud K, Sopp
545 P, Nakanishi M, Bowden R, Cowley S, Newey S, Akerman C, Ponting CP, Cader MZ.
546 Assessing similarity to primary tissue and cortical layer identity in induced
547 pluripotent stem cell-derived cortical neurons through single-cell transcriptomics.
548 *Human Molecular Genetics.* 2016; 25(5):989-1000.
549 **11.** Osorio D, Cai JJ. Systematic determination of the mitochondrial proportion in human
550 and mice tissues for single-cell RNA-sequencing data quality control. *Bioinformatics.*
551 2021; 37(7):963-967.
552 **12.** Hao Y, Hao S, Andersen-Nissen E, Mauck WM, 3rd, Zheng S, Butler A, Lee MJ, Wilk AJ,
553 Darby C, Zager M, Hoffman P, Stoeckius M, Papalexi E, Mimitou EP, Jain J, Srivastava
554 A, Stuart T, Fleming LM, Yeung B, Rogers AJ, McElrath JM, Blish CA, Gottardo R,
555 Smibert P, Satija R. Integrated analysis of multimodal single-cell data. *Cell.* 2021;
556 184(13):3573-3587 e3529.
557 **13.** Korsunsky I, Nathan A, Millard N, Raychaudhuri S. Presto scales Wilcoxon and auROC
558 analyses to millions of observations. *bioRxiv.* 2019:653253.
559 **14.** Liberzon A, Birger C, Thorvaldsdóttir H, Ghandi M, Mesirov JP, Tamayo P. The
560 Molecular Signatures Database (MSigDB) hallmark gene set collection. *Cell Syst.*
561 2015; 1(6):417-425.
562 **15.** Sergushichev AA. An algorithm for fast preranked gene set enrichment analysis using
563 cumulative statistic calculation. *bioRxiv.* 2016:060012.
564 **16.** Kolberg L, Raudvere U, Kuzmin I, Adler P, Vilo J, Peterson H. g:Profiler—interoperable
565 web service for functional enrichment analysis and gene identifier mapping (2023
566 update). *Nucleic Acids Research.* 2023; 51(W1):W207-W212.
567 **17.** Shannon P, Markiel A, Ozier O, Baliga NS, Wang JT, Ramage D, Amin N, Schwikowski
568 B, Ideker T. Cytoscape: a software environment for integrated models of
569 biomolecular interaction networks. *Genome Res.* 2003; 13(11):2498-2504.
570 **18.** Cao J, Spielmann M, Qiu X, Huang X, Ibrahim DM, Hill AJ, Zhang F, Mundlos S,
571 Christiansen L, Steemers FJ, Trapnell C, Shendure J. The single-cell transcriptional
572 landscape of mammalian organogenesis. *Nature.* 2019; 566(7745):496-502.
573 **19.** Haghverdi L, Lun ATL, Morgan MD, Marioni JC. Batch effects in single-cell RNA-
574 sequencing data are corrected by matching mutual nearest neighbors. *Nat*
575 *Biotechnol.* 2018; 36(5):421-427.
576 **20.** Laura MR, Mazdak R, Suluxan M, Shamini A, Danielle CC, Díaz-Mejía JJ, Fiona JC,
577 Peter BD, Trevor JP. A comparison of data integration methods for single-cell RNA
578 sequencing of cancer samples. *bioRxiv.* 2021:2021.2008.2004.453579.

579 **21.** Schäfer M, Werner S. Cancer as an overhealing wound: an old hypothesis revisited.
580 *Nat Rev Mol Cell Biol.* 2008; 9(8):628-638.
581 **22.** Nguyen LXT, Raval A, Garcia JS, Mitchell BS. Regulation of Ribosomal Gene
582 Expression in Cancer. *Journal of Cellular Physiology.* 2015; 230(6):1181-1188.
583 **23.** Janiszewska M, Primi MC, Izard T. Cell adhesion in cancer: Beyond the migration of
584 single cells. *J Biol Chem.* 2020; 295(8):2495-2505.
585 **24.** Owa T, Taya S, Miyashita S, Yamashita M, Adachi T, Yamada K, Yokoyama M, Aida S,
586 Nishioka T, Inoue YU, Goitsuka R, Nakamura T, Inoue T, Kaibuchi K, Hoshino M.
587 Meis1 Coordinates Cerebellar Granule Cell Development by Regulating Pax6
588 Transcription, BMP Signaling and Atoh1 Degradation. *J Neurosci.* 2018; 38(5):1277-
589 1294.
590 **25.** Machold R, Klein C, Fishell G. Genes expressed in Atoh1 neuronal lineages arising
591 from the r1/isthmus rhombic lip. *Gene Expr Patterns.* 2011; 11(5-6):349-359.
592 **26.** Xu X, Stoyanova EI, Lemiesz AE, Xing J, Mash DC, Heintz N. Species and cell-type
593 properties of classically defined human and rodent neurons and glia. *Elife.* 2018; 7.
594 **27.** Bizzoca A, Virgintino D, Lorusso L, Buttiglione M, Yoshida L, Polizzi A, Tattoli M,
595 Cagiano R, Rossi F, Kozlov S, Furley A, Gennarini G. Transgenic mice expressing
596 F3/contactin from the TAG-1 promoter exhibit developmentally regulated changes in
597 the differentiation of cerebellar neurons. *Development.* 2003; 130(1):29-43.
598 **28.** Nayler S, Agarwal D, Curion F, Bowden R, Becker EBE. High-resolution transcriptional
599 landscape of xeno-free human induced pluripotent stem cell-derived cerebellar
600 organoids. *Scientific Reports.* 2021; 11(1):12959.
601 **29.** Miyata T, Maeda T, Lee JE. NeuroD is required for differentiation of the granule cells
602 in the cerebellum and hippocampus. *Genes Dev.* 1999; 13(13):1647-1652.
603 **30.** Behesti H, Kocabas A, Buchholz DE, Carroll TS, Hatten ME. Altered temporal
604 sequence of transcriptional regulators in the generation of human cerebellar granule
605 cells. *eLife.* 2021; 10:e67074.
606 **31.** Hovestadt V, Smith KS, Bihannic L, Filbin MG, Shaw ML, Baumgartner A, DeWitt JC,
607 Groves A, Mayr L, Weisman HR, Richman AR, Shore ME, Goumnerova L, Rosencrance
608 C, Carter RA, Phoenix TN, Hadley JL, Tong Y, Houston J, Ashmun RA, DeCuypere M,
609 Sharma T, Flasch D, Silkov A, Ligon KL, Pomeroy SL, Rivera MN, Rozenblatt-Rosen O,
610 Rusert JM, Wechsler-Reya RJ, Li X-N, Peyrl A, Gojo J, Kirchhofer D, Lötsch D, Czech T,
611 Dorfer C, Haberler C, Geyeregger R, Halfmann A, Gawad C, Easton J, Pfister SM,
612 Regev A, Gajjar A, Orr BA, Slavc I, Robinson GW, Bernstein BE, Suvà ML, Northcott
613 PA. Resolving medulloblastoma cellular architecture by single-cell genomics. *Nature.*
614 2019; 572(7767):74-79.
615 **32.** Riemondy KA, Venkataraman S, Willard N, Nellan A, Sanford B, Griesinger AM, Amani
616 V, Mitra S, Hankinson TC, Handler MH, Sill M, Ocasio J, Weir SJ, Malawsky DS,
617 Gershon TR, Garancher A, Wechsler-Reya RJ, Hesselberth JR, Foreman NK, Donson
618 AM, Vibhakar R. Neoplastic and immune single-cell transcriptomics define subgroup-
619 specific intra-tumoral heterogeneity of childhood medulloblastoma. *Neuro Oncol.*
620 2022; 24(2):273-286.
621 **33.** Brotto DB, Siena ÁDD, de Barros II, Carvalho SdCeS, Muys BR, Goedert L, Cardoso C,
622 Plaça JR, Ramão A, Squire JA, Araujo LF, Silva WAd. Contributions of HOX genes to
623 cancer hallmarks: Enrichment pathway analysis and review. *Tumor Biology.* 2020;
624 42(5):1010428320918050.

625 **34.** Zhang H, Zheng J, Fu Y, Ling J, Liu Z, Lin X, Dong X, Sun Y, Tan T, Guo Z, Xie G.
626 Overexpression of POU3F2 promotes radioresistance in triple-negative breast cancer
627 via Akt pathway activation. *Breast Cancer Research and Treatment.* 2023;
628 198(3):437-446.
629 **35.** Tomoo O, Shinichiro T, Satoshi M, Mariko Y, Toma A, Koyo Y, Miwa Y, Shogo A,
630 Tomoki N, Yukiko UI, Ryo G, Takuro N, Takayoshi I, Kozo K, Mikio H. Meis1
631 Coordinates Cerebellar Granule Cell Development by Regulating Pax6 Transcription,
632 BMP Signaling and Atoh1 Degradation. *The Journal of Neuroscience.* 2018;
633 38(5):1277.
634 **36.** Shao W, Ding Q, Guo Y, Xing J, Huo Z, Wang Z, Xu Q, Guo Y. A Pan-Cancer Landscape
635 of HOX-Related lncRNAs and Their Association With Prognosis and Tumor
636 Microenvironment. *Front Mol Biosci.* 2021; 8:767856.
637 **37.** Tantin D. Oct transcription factors in development and stem cells: insights and
638 mechanisms. *Development.* 2013; 140(14):2857-2866.
639 **38.** Yuzwa SA, Borrett MJ, Innes BT, Voronova A, Ketela T, Kaplan DR, Bader GD, Miller
640 FD. Developmental Emergence of Adult Neural Stem Cells as Revealed by Single-Cell
641 Transcriptional Profiling. *Cell Reports.* 2017; 21(13):3970-3986.
642 **39.** Vanner RJ, Remke M, Gallo M, Selvadurai HJ, Coutinho F, Lee L, Kushida M, Head R,
643 Morrissy S, Zhu X, Aviv T, Voisin V, Clarke ID, Li Y, Mungall AJ, Moore RA, Ma Y, Jones
644 SJ, Marra MA, Malkin D, Northcott PA, Kool M, Pfister SM, Bader G, Hochedlinger K,
645 Korshunov A, Taylor MD, Dirks PB. Quiescent sox2(+) cells drive hierarchical growth
646 and relapse in sonic hedgehog subgroup medulloblastoma. *Cancer Cell.* 2014;
647 26(1):33-47.
648 **40.** Bertolini J, Mercurio S, Favaro R, Mariani J, Ottolenghi S, Nicolis SK. Sox2-Dependent
649 Regulation of Neural Stem Cells and CNS Development. In: Kondoh H, Lovell-Badge R,
650 eds. *Sox2: Biology and Role in Development and Disease*: Academic Press; 2016:187-
651 216.
652 **41.** Lun ATL. A description of the theory behind the fastMNN algorithm. 2019;
653 https://marionilab.github.io/FurtherMNN2018/theory/description.html.
654 **42.** Stuart T, Butler A, Hoffman P, Hafemeister C, Papalexi E, Mauck WM, 3rd, Hao Y,
655 Stoeckius M, Smibert P, Satija R. Comprehensive Integration of Single-Cell Data. *Cell.*
656 2019; 177(7):1888-1902 e1821.
657 **43.** Essen MJv, Riepsaame J, Cowley SA, Jacob J, Becker EBE. PTCH1 mutant human
658 cerebellar organoids are associated with altered neural development and early
659 pathways of medulloblastoma oncogenesis. *bioRxiv.* 2023:2023.2005.2010.540200.
660 **44.** Vladoiu MC, El-Hamamy I, Donovan LK, Farooq H, Holgado BL, Sundaravadanam Y,
661 Ramaswamy V, Hendrikse LD, Kumar S, Mack SC, Lee JJY, Fong V, Juraschka K,
662 Przelicki D, Michealraj A, Skowron P, Luu B, Suzuki H, Morrissy AS, Cavalli FMG,
663 Garzia L, Daniels C, Wu X, Qazi MA, Singh SK, Chan JA, Marra MA, Malkin D, Dirks P,
664 Heisler L, Pugh T, Ng K, Notta F, Thompson EM, Kleinman CL, Joyner AL, Jabado N,
665 Stein L, Taylor MD. Childhood cerebellar tumours mirror conserved fetal
666 transcriptional programs. *Nature.* 2019; 572(7767):67-73.
667 **45.** Smith BA, Balanis NG, Nanjundiah A, Sheu KM, Tsai BL, Zhang Q, Park JW, Thompson
668 M, Huang J, Witte ON, Graeber TG. A Human Adult Stem Cell Signature Marks
669 Aggressive Variants across Epithelial Cancers. *Cell Rep.* 2018; 24(12):3353-
670 3366.e3355.

671 **46.** Cheng Y, Liao S, Xu G, Hu J, Guo D, Du F, Contreras A, Cai KQ, Peri S, Wang Y, Corney
672 DC, Noronha AM, Chau LQ, Zhou G, Wiest DL, Bellacosa A, Wechsler-Reya RJ, Zhao Y,
673 Yang ZJ. NeuroD1 Dictates Tumor Cell Differentiation in Medulloblastoma. *Cell Rep.*
674 2020; 31(12):107782.
675 **47.** Ocasio JK, Babcock B, Malawsky D, Weir SJ, Loo L, Simon JM, Zylka MJ, Hwang D,
676 Dismuke T, Sokolsky M, Rosen EP, Vibhakar R, Zhang J, Saulnier O, Vladoiu M, El-
677 Hamamy I, Stein LD, Taylor MD, Smith KS, Northcott PA, Colaneri A, Wilhelmsen K,
678 Gershon TR. scRNA-seq in medulloblastoma shows cellular heterogeneity and
679 lineage expansion support resistance to SHH inhibitor therapy. *Nat Commun.* 2019;
680 10(1):5829.
681 **48.** Oh L, Hafsi H, Hainaut P, Ariffin H. p53, stem cell biology and childhood blastomas.
682 *Current Opinion in Oncology.* 2019; 31(2).
683 **49.** Wang M, Zhao J, Zhang L, Wei F, Lian Y, Wu Y, Gong Z, Zhang S, Zhou J, Cao K, Li X,
684 Xiong W, Li G, Zeng Z, Guo C. Role of tumor microenvironment in tumorigenesis.
685 *Journal of Cancer.* 2017; 8(5):761-773.
686 **50.** Pickup MW, Mouw JK, Weaver VM. The extracellular matrix modulates the hallmarks
687 of cancer. *EMBO Rep.* 2014; 15(12):1243-1253.
688

689

# Figure 1

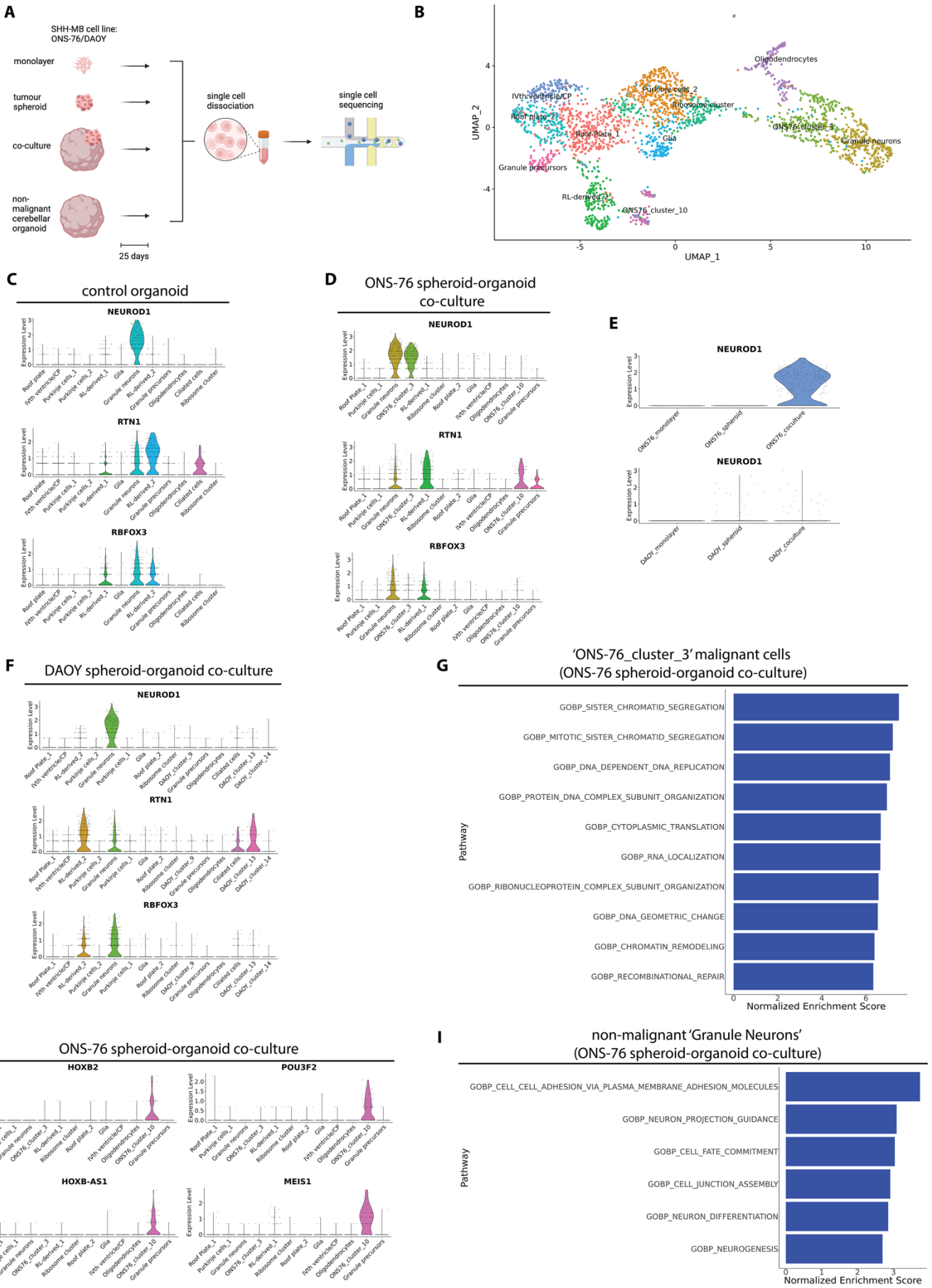
A
SHH-MB cell line:
ONS-76/DAOY
monolayer
tumour spheroid
co-culture
non-malignant cerebellar organoid
25 days
single cell dissociation
single cell sequencing
B
UMAP_2
UMAP_1
Oligodendrocytes
IVth ventricle/CP
Purkinje cells_2
Ribosome cluster
Roof plate_2
Roof Plate_1
Glia
ONS76_cluster_3
Granule neurons
Granule precursors
RL-derived_2
ONS76_cluster_10
C
control organoid
NEUROD1
RTN1
RBFOX3
Expression Level
D
ONS-76 spheroid-organoid co-culture
NEUROD1
RTN1
RBFOX3
E
NEUROD1
ONS76_monolayer
ONS76_spheroid
ONS76_coculture
NEUROD1
DAOY_monolayer
DAOY_spheroid
DAOY_coculture
F
DAOY spheroid-organoid co-culture
NEUROD1
RTN1
RBFOX3
G
'ONS-76_cluster_3' malignant cells
(ONS-76 spheroid-organoid co-culture)
GOBP_SISTER_CHROMATID_SEGREGATION
GOBP_MITOTIC_SISTER_CHROMATID_SEGREGATION
GOBP_DNA_DEPENDENT_DNA_REPLICATION
GOBP_PROTEIN_DNA_COMPLEX_SUBUNIT_ORGANIZATION
GOBP_CYTOPLASMIC_TRANSLATION
GOBP_RNA_LOCALIZATION
GOBP_RIBONUCLEOPROTEIN_COMPLEX_SUBUNIT_ORGANIZATION
GOBP_DNA_GEOMETRIC_CHANGE
GOBP_CHROMATIN_REMODELING
GOBP_RECOMBINATIONAL_REPAIR
Pathway
Normalized Enrichment Score
H
ONS-76 spheroid-organoid co-culture
HOXB2
POU3F2
HOXB-AS1
MEIS1
I
non-malignant 'Granule Neurons'
(ONS-76 spheroid-organoid co-culture)
GOBP_CELL_CELL_ADHESION_VIA_PLASMA_MEMBRANE_ADHESION_MOLECULES
GOBP_NEURON_PROJECTION_GUIDANCE
GOBP_CELL_FATE_COMMITMENT
GOBP_CELL_JUNCTION_ASSEMBLY
GOBP_NEURON_DIFFERENTIATION
GOBP_NEUROGENESIS
Pathway
Normalized Enrichment Score

690

691 **Figure 1**. Upregulation of *NEUROD1* in ONS-76 cells in co-culture compared to monolayer or
692 tumour spheroid growth conditions. (A) Schematic of experimental workflow. This figure
693 was created with BioRender.com. (B) UMAP visualisation of single-cell transcriptomes of
694 ONS-76 cells in co-culture identified two malignant cell clusters annotated as
695 'ONS76_cluster_3' and 'ONS76_cluster_10'. (C) Violin plot showing co-expression of
696 *NEUROD1*, *RTN1* and *RBFOX3* in the 'Granule neurons' cluster of the control organoid. (D)
697 Violin plot of expression of *NEUROD1,* and absent *RTN1* and *RBFOX3* expression in
698 'ONS76_cluster_3' in the ONS-76 tumour spheroid-organoid co-culture (E) Violin plots of the
699 expression of *NEUROD1* in ONS-76 cells (upper panel) and DAOY cells (lower panel) grown
700 as monolayers, tumour spheroids or in tumour spheroid-organoid co-culture. (F) Expression
701 of *NEUROD1* in the DAOY tumour spheroid-organoid co-culture sample is restricted to the
702 non-malignant 'Granule neurons' cluster. (G) fgsea gene set enrichment of upregulated gene
703 ontology (GO) biological pathway terms evaluated by normalised enrichment scores of the
704 *NEUROD1*+ cluster of malignant cells ('ONS76_cluster_3') in the ONS-76 tumour spheroid-
705 organoid co-culture sample. (H) Violin plot of marker genes of the second malignant cluster,
706 'ONS76_cluster_10' in the ONS-76 tumour spheroid-organoid co-culture sample. (I) fgsea
707 gene set enrichment of upregulated GO biological pathway terms evaluated by normalised
708 enrichment scores of non-malignant *NEUROD1*+ cells ('Granule neurons') in the ONS-76
709 tumour spheroid-organoid co-culture sample.
710
711
712

## Figure 2

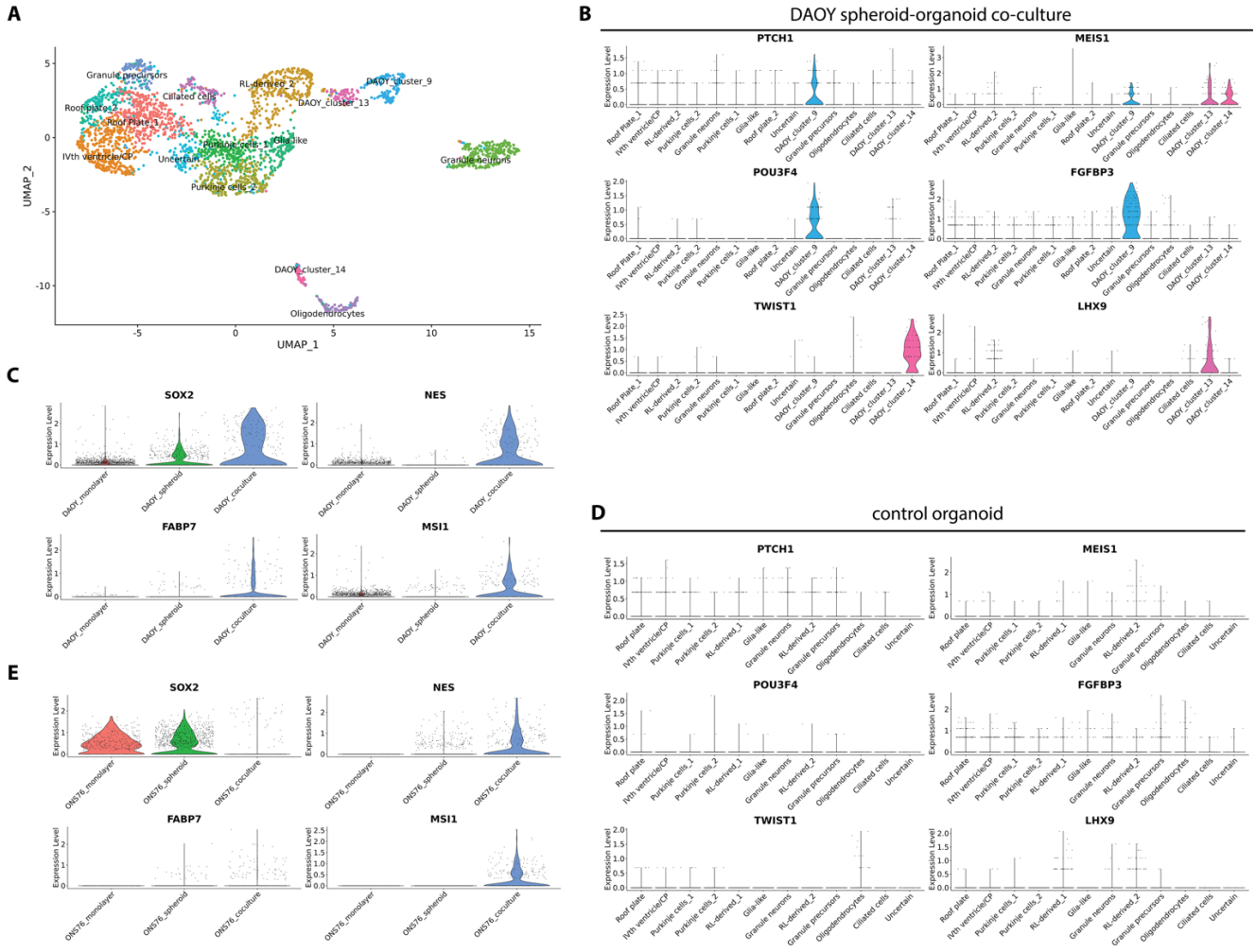


**Figure 2**. Upregulation of neural stem cell markers in DAOY malignant cells in co-culture. (A) UMAP visualisation of single-cell transcriptomes in DAOY tumour spheroid-organoid co-cultures shows three malignant clusters annotated as 'DAOY_cluster_9, 'DAOY_cluster_13' and 'DAOY_cluster_14'. (B) Violin plots showing expression of unique markers of malignant DAOY clusters in co-culture. (C) Violin plots of expression of the indicated neural stem cell markers in DAOY cells in tumour spheroid-organoid co-culture, tumour spheroid and monolayer cultures. (D) Expression of the indicated genes in cells of the control organoid sample. (E) Violin plots of expression of the indicated neural stem cell markers in ONS-76 cells in tumour spheroid-organoid co-culture, tumour spheroid and monolayer cultures.

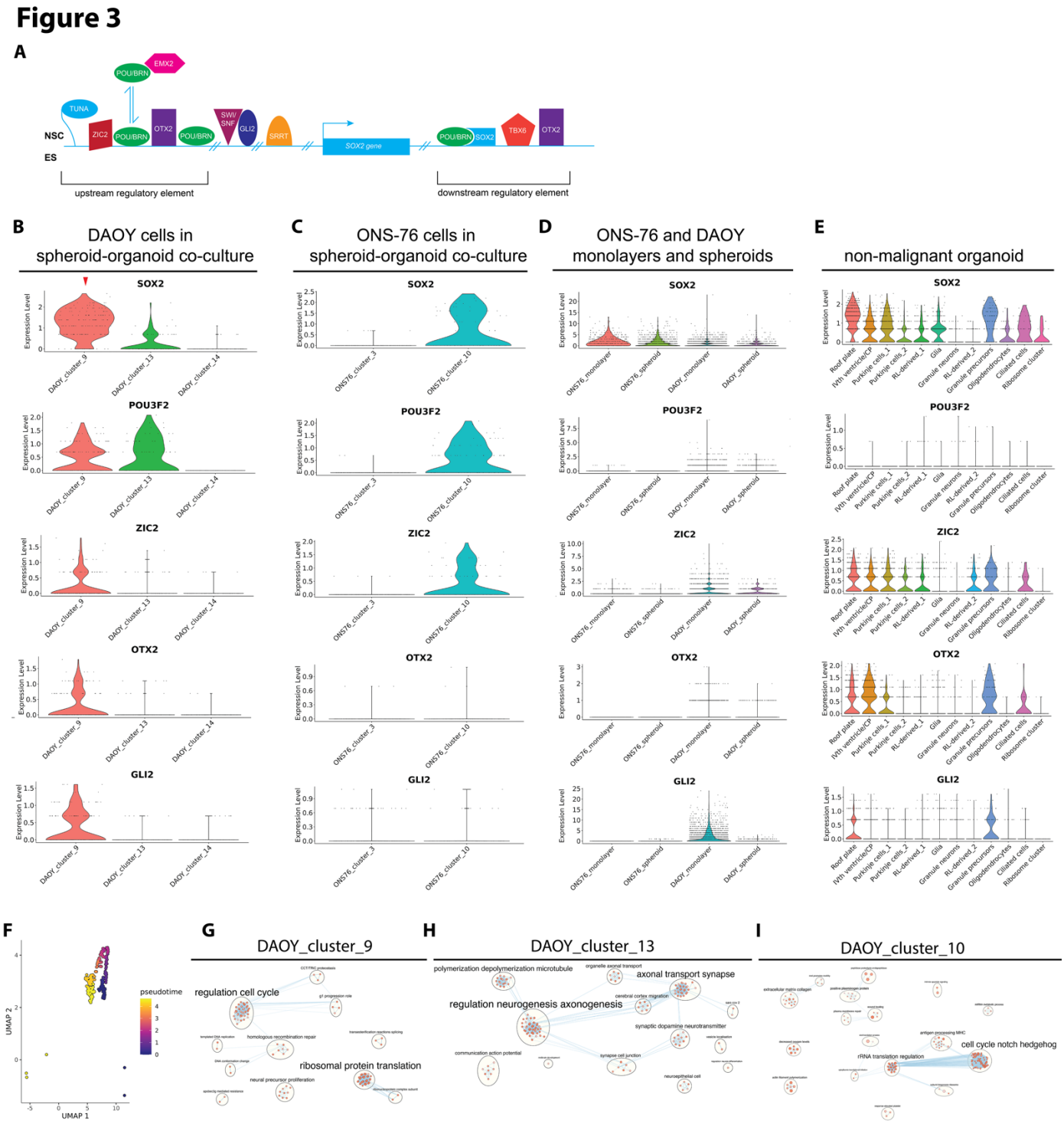


**Figure 3**. Multiple factors known to regulate the expression of *SOX2* in NSC and ES cells (ESC) are also expressed in a sub-population of DAOY cells in co-culture. (A) Schematic of the *SOX2* regulatory network in NSC and ESC (adapted from Bertolini et al.[40]). (B) Violin plots of expression of the *SOX2* regulatory network in 'DAOY_cluster_9' cells. (C) Expression of a sparse *SOX2* regulatory network in ONS-76 cells in tumour spheroid-organoid co-culture. (D) *SOX2* regulatory network expression in DAOY and ONS-76 monolayer and tumour spheroid

732 cultures. (E) Gene expression of the *SOX2* regulatory network in non-malignant organoids.
733 (F) Pseudotime trajectory of cells in 'DAOY_cluster_9'. (G) Enrichment of GO biological
734 pathway terms upregulated in 'DAOY_cluster_9' visualised in Cytoscape.[17] (H) Enrichment of
735 GO biological pathway terms upregulated in 'DAOY_cluster_13' visualised in Cytoscape. (I)
736 Enrichment of GO biological pathway terms upregulated in 'DAOY_cluster_10' visualised in
737 Cytoscape. *TBX6* was not expressed in malignant cells.
738
739

## Figure 4

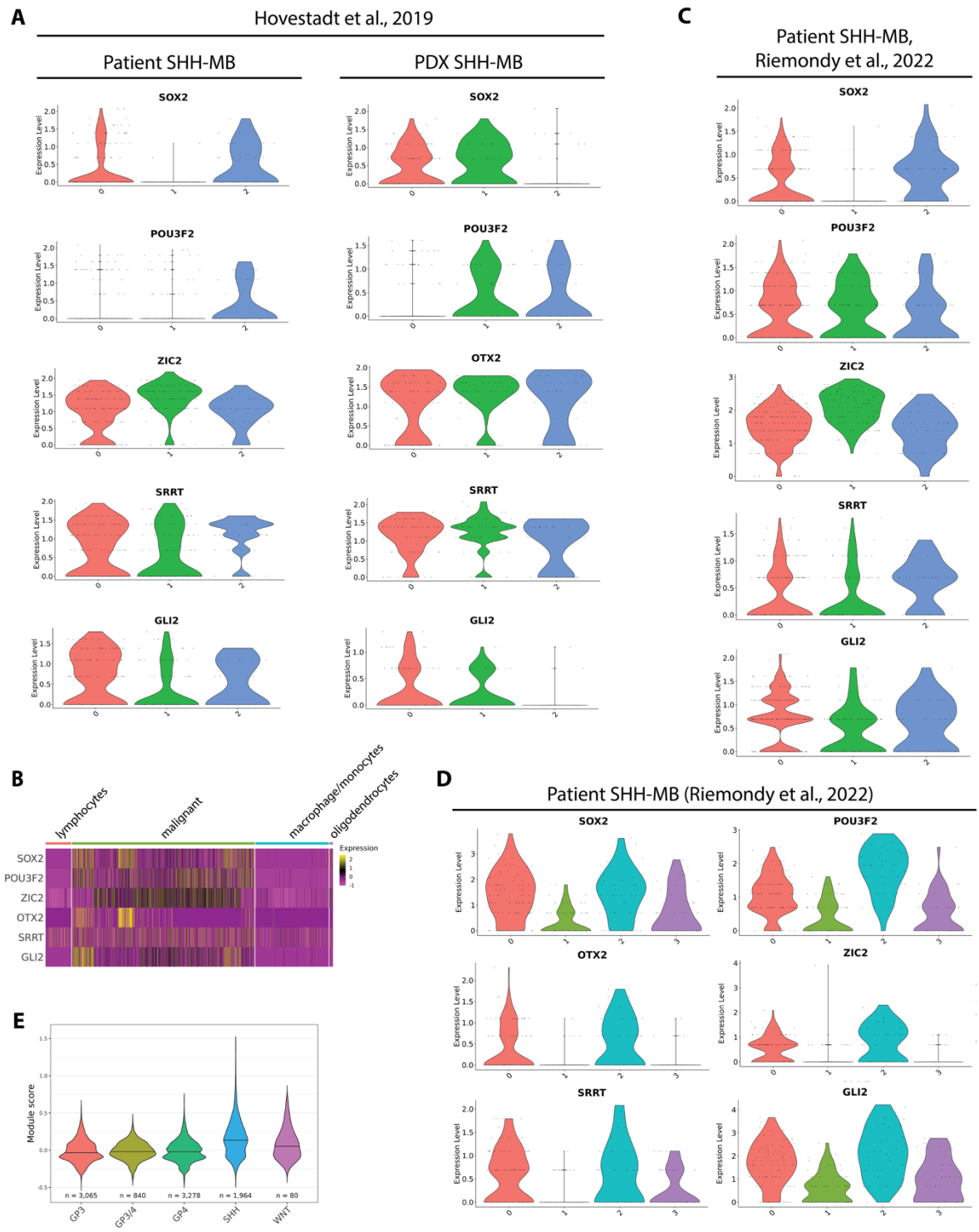


**Figure 4**.

Expression of the *SOX2* regulatory network in patient SHH-MB datasets sequenced at single-cell level. (A) Violin plots of the expression of the *SOX2* regulatory network in one of three patient SHH-MB (tumour ID: SJ454) and in a SHH-MB PDX tumour model (tumour ID: RMCB18) from the same dataset.[31] (B) Heatmap of expression of the *SOX2* regulatory

746 network in malignant cells and in cells of the microenvironment in a second patient SHH-MB
747 dataset.[32] Cell labels are retained from the original publication. (C) Expression of the *SOX2*
748 regulatory network in two of three UMAP clusters in a patient tumour (tumour ID: 1235)
749 from the same dataset.[32] (D) *SOX2* regulatory network expression in another tumour
750 (tumour ID: 801) from the same dataset.[32] (E) Violin plots of cell scores for the *SOX2*
751 regulatory network in all medulloblastoma subtypes. Only malignant cells are included.[32] For
752 malignant cell numbers in each SHH-MB see Supplementary Fig. S4. *TBX6* was not expressed
753 in malignant cells in either dataset.
754
755
756
757
758

**Figure 5**

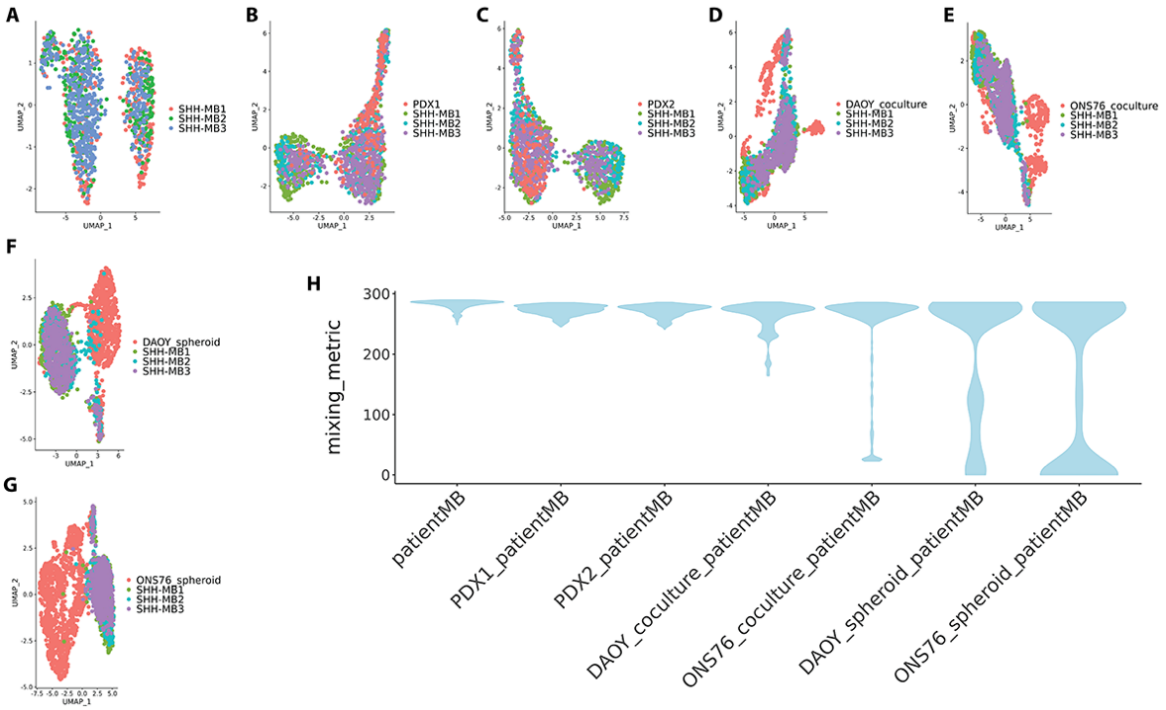


759
760 **Figure 5**. The co-culture tumour models recapitulate SHH-MB patient tumours better than
761 conventional *in vitro* models. (A) UMAP visualisation of three SHH-MB patient tumours. (B)
762 Integration and UMAP visualisation of cells from a PDX SHH-MB tumour (PDX1) with the
763 same three SHH-MB patient tumours as in A. (C) Integration and UMAP visualisation of cells
764 from a second PDX SHH-MB tumour (PDX2) with the three SHH-MB patient tumours. (D)

765 Integration and UMAP visualisation of DAOY cells in tumour spheroid-organoid co-culture
766 with the three SHH-MB patient tumours. (E) Integration and UMAP visualisation of ONS-76
767 cells in tumour spheroid-organoid co-culture with the three patient SHH-MB tumours. (F)
768 Integration and UMAP visualisation of DAOY tumour spheroid cells with the three patient
769 SHH-MB tumours. (G) Integration and UMAP visualisation of ONS-76 tumour spheroid cells
770 with the three patient SHH-MB tumours. (H) Violin plots of mixing metric scores of the
771 integrations shown in A to G. Patient and PDX tumour datasets were obtained from the
772 published study by Hovestadt et al.[31] Only malignant cells were used for scoring.
773
774
775